



1 **Impact of anthropogenic emissions on biogenic secondary**  
2 **organic aerosol: Observation in the Pearl River Delta,**  
3 **South China**

4 Yu-Qing Zhang<sup>1, \*</sup>, Duo-Hong Chen<sup>2, \*</sup>, Xiang Ding<sup>1, †</sup>, Jun Li<sup>1</sup>, Tao Zhang<sup>2</sup>, Jun-Qi  
5 Wang<sup>1</sup>, Qian Cheng<sup>1</sup>, Hao Jiang<sup>1</sup>, Wei Song<sup>1</sup>, Yu-Bo Ou<sup>2</sup>, Peng-Lin Ye<sup>3</sup>, Gan Zhang<sup>1</sup>,  
6 Xin-Ming Wang<sup>1, 4</sup>

7 1 State Key Laboratory of Organic Geochemistry and Guangdong Provincial Key Laboratory of  
8 Environmental Protection and Resources Utilization, Guangzhou Institute of Geochemistry, Chinese  
9 Academy of Sciences, Guangzhou, 510640, China

10 2 State Environmental Protection Key Laboratory of Regional Air Quality Monitoring, Environmental  
11 Monitoring Center of Guangdong Province, Guangzhou, 510308, China

12 3 Aerodyne Research Inc., Billerica, Massachusetts 01821, United States

13 4 Center for Excellence in Regional Atmospheric Environment, Institute of Urban Environment, Chinese  
14 Academy of Sciences, Xiamen, 361021, China

15 \* These authors contributed equally to this work.

16 † Correspondence to: Xiang Ding (xiangd@gig.ac.cn)

17



18 **Abstract.** Secondary organic aerosol (SOA) formation from biogenic precursors is affected by  
19 anthropogenic emissions, which is not well understood in polluted areas. In the study, we accomplished  
20 a year-round campaign at nine sites in the polluted areas located in Pearl River Delta (PRD) region during  
21 2015. We measured typical biogenic SOA (BSOA) tracers from isoprene, monoterpenes, and  $\beta$ -  
22 caryophyllene as well as major gaseous and particulate pollutants and investigated the impact of  
23 anthropogenic pollutants on BSOA formation. The concentrations of BSOA tracers were in the range of  
24 45.4 to 109 ng m<sup>-3</sup> with the majority composed of products from monoterpenes (SOA<sub>M</sub>, 47.2 ± 9.29 ng  
25 m<sup>-3</sup>), followed by isoprene (SOA<sub>I</sub>, 23.1 ± 10.8 ng m<sup>-3</sup>), and  $\beta$ -caryophyllene (SOA<sub>C</sub>, 3.85 ± 1.75 ng m<sup>-3</sup>).  
26 We found that atmospheric oxidants, O<sub>x</sub> (O<sub>3</sub> plus NO<sub>2</sub>), and sulfate correlated well with high-generation  
27 SOA<sub>M</sub> tracers, but not so for first-generation SOA<sub>M</sub> products. This suggested that high O<sub>x</sub> and sulfate  
28 could promote the formation of high-generation SOA<sub>M</sub> products, which probably led to relatively aged  
29 SOA<sub>M</sub> we observed in the PRD. For the SOA<sub>I</sub> tracers, not only 2-methylglyceric acid (NO/NO<sub>2</sub>-channel  
30 product), but also the ratio of 2-methylglyceric acid to 2-methyltetrols (HO<sub>2</sub>-channel products) exhibit  
31 NO<sub>x</sub> dependence, indicating the significant impact of NO<sub>x</sub> on SOA<sub>I</sub> formation pathways. The SOA<sub>C</sub> tracer  
32 elevated in winter at all sites and positively correlated with levoglucosan, O<sub>x</sub>, and sulfate. Thus, the  
33 unexpected increase of SOA<sub>C</sub> in wintertime might be highly associated with the enhancement of biomass  
34 burning, atmospheric oxidation capacity and sulfate components in the PRD. The BSOAs that were  
35 estimated by the SOA tracer approach showed the highest concentration in fall and the lowest  
36 concentration in spring with an annual average concentration of 1.68 ± 0.40 μg m<sup>-3</sup>. SOA<sub>M</sub> dominated  
37 the BSOA mass all year round. We also found that BSOA correlated well with sulfate and O<sub>x</sub>. This  
38 implicated the significant effects of anthropogenic pollutants on BSOA formation and highlighted that  
39 we could reduce the BSOA through controlling on the anthropogenic emissions of sulfate and O<sub>x</sub>  
40 precursors in polluted regions.

## 41 **1 Introduction**

42 Secondary organic aerosols (SOA) that are produced through homogenous and heterogeneous processes  
43 of volatile organic compounds (VOCs) have significant effects on global climate change and regional air  
44 quality (von Schneidmesser et al., 2015). Globally, the emissions of biogenic VOCs (BVOCs) are  
45 dominant over anthropogenic VOCs. Thus, biogenic SOA (BSOA) is predominant over anthropogenic



46 SOA. In the past decade, laboratorial, field, and modeling studies have demonstrated that BSOA  
47 formation is highly affected by anthropogenic emissions (Zhang et al., 2015; Hoyle et al., 2011; Carlton  
48 et al., 2010). Increasing  $\text{NO}_x$  shifts isoprene oxidation from the low- $\text{NO}_x$  conditions to the high- $\text{NO}_x$   
49 conditions (Surratt et al., 2010) and enhances nighttime SOA formation via nitrate radical oxidation of  
50 monoterpenes (Xu et al., 2015). High  $\text{SO}_2$  emission leads to abundant sulfate and acidic particles, which  
51 accelerates the BSOA production by the salting-in effect and acid-catalyzed reactions (Offenberg et al.,  
52 2009; Xu et al., 2016). In polluted regions, the increase of  $\text{O}_3$  levels due to high emissions of  $\text{NO}_x$  and  
53 VOCs, likely results in significant SOA formation through the ozonolysis of BVOCs (Sipilä et al., 2014;  
54 Riva et al., 2017). In addition, large emission and formation of anthropogenic organic matter (OM) in  
55 urban areas enhance the incorporation of BVOCs' oxidation products into the condensed phase (Donahue  
56 et al., 2006). Recently, Carlton et al. (2018) found that the removal of anthropogenic emissions of  $\text{NO}_x$ ,  
57  $\text{SO}_2$ , and primary OA in the CMAQ simulations could reduce BSOA by 23, 14, and 8% in summertime,  
58 respectively.

59 The Pearl River Delta region (PRD) (Figure 1a) is the most developed region in China. Rapid  
60 economic growth during the past three decades has resulted in large amounts of anthropogenic emissions  
61 in the PRD (Lu et al., 2013). Our observation during fall-winter season in 2008 at a regional site of the  
62 PRD showed that daily  $\text{PM}_{2.5}$  was as high as  $150 \mu\text{g m}^{-3}$  (Ding et al., 2012). Fortunately, due to more and  
63 more strict and effective pollution controls in the PRD,  $\text{PM}_{2.5}$  concentrations have significantly shrunk  
64 during the last decade and met the national ambient air quality standard (NAAQS) for annual-mean  $\text{PM}_{2.5}$   
65 ( $35 \mu\text{g m}^{-3}$ ) since the year of 2015 (Figure 1b). However,  $\text{O}_3$  and oxidant ( $\text{O}_x$ ,  $\text{O}_x = \text{O}_3 + \text{NO}_2$ ) are still in  
66 high levels and do not decrease apparently (Figure 1b), indicating that atmospheric oxidative capacity in  
67 the PRD is still high (Hofzumahaus et al., 2009). On the other hand, BVOCs emissions in the PRD are  
68 expected to be high all the year in such a subtropical area (Zheng et al., 2010). In the process of such a  
69 dramatic change in air pollution characteristics (e.g.  $\text{PM}_{2.5}$  and  $\text{O}_3$ ), BSOA origins and formation  
70 mechanisms in the PRD should be profoundly affected in the last decade. In this study, year-round  $\text{PM}_{2.5}$   
71 samples were collected at nine sites in the PRD during 2015. We investigated SOA tracers from typical  
72 BVOCs (isoprene, monoterpenes, and  $\beta$ -caryophyllene) across the PRD for the first time. We checked  
73 seasonal variations in concentrations and compositions of these BSOA tracers and evaluated the impact  
74 of anthropogenic pollutants on BSOAs formation in the PRD. We also accessed the SOA origins and  
75 discussed the implication in further reducing BSOA through controlling on the anthropogenic emissions.



## 76 2 Experimental Section

### 77 2.1 Field Sampling

78 Concurrent sampling was performed at 9 out of 23 sites in the Guangdong-Hong Kong-Macao regional  
79 air quality monitoring network (<http://www.gdep.gov.cn/hjjce/>, Figure 1a), including three urban sites in  
80 Zhaoqing (ZQ), Guangzhou (GZ) and Dongguan (DG), two suburban sites in Nansha (NS) and Zhuhai  
81 (ZH), and four rural sites in Tianhu (TH), Boluo (BL), Heshan (HS) and Taishan (TS).

82 At each site, 24-hr sampling was conducted every six days from January to December in 2015 using  
83 a PM<sub>2.5</sub> sampler equipped with quartz filters (8 × 10 inches) at a flow rate of 1.1 m<sup>3</sup> min<sup>-1</sup>. Additionally,  
84 field blanks were collected monthly at all sites. Blank filters were covered with aluminum foil and baked  
85 at 500 °C for 12 hrs and stored in a container with silica gel. After sampling, the filter samples were  
86 stored at -20 °C.

87 In this study, the filters collected in January, April, July and October 2015 were selected to represent  
88 winter, spring, summer, and fall samples, respectively. A total of 170 field samples (4-5 samples for each  
89 season at each site) were analyzed in the current study.

### 90 2.2 Chemical Analysis

91 For each filter, organic carbon (OC) and elemental carbon (EC) were measured by an OC-EC aerosol  
92 analyzer (Sunset Laboratory Inc.). Water-soluble ions were analyzed by ion chromatography (Metrohm).  
93 All these species are major components in PM<sub>2.5</sub> (see Figure 2). Meteorological parameters (temperature  
94 and relative humidity) and gaseous pollutants (SO<sub>2</sub>, CO, NO<sub>2</sub>, NO, and O<sub>3</sub>) at each site were recorded  
95 hourly. We further calculated the daily averages to probe the potential influence of air pollutants on  
96 BSOA formation.

97 For BSOA tracer analysis, detailed information of the processes is described in the previous  
98 literatures (Shen et al., 2015; Ding et al., 2012). Isotope-labeled standard mixtures, including dodecanoic  
99 acid-d<sub>23</sub>, hexadecanoic acid-d<sub>31</sub>, docosanoic acid-d<sub>43</sub> and levoglucosan-<sup>13</sup>C<sub>6</sub> were added into each sample  
100 as internal standards. Then, samples were extracted by sonication with the mixed solvents of dichloride  
101 methane (DCM)/hexane (1:1, v/v) and DCM/methanol (1:1, v/v), sequentially. The extraction solutions  
102 of each sample were combined, filtered, and concentrated to ~2 mL. Each concentrated sample was split  
103 into two parts for silylation and methylation, respectively.

104 We analyzed fourteen BSOA tracers in the derivatized samples using GC/MSD (Agilent



105 7890/5975C). The isoprene-derived SOA (SOA<sub>I</sub>) tracers were composed of 2-methylglyceric acid (2-  
106 MGA), 2-methyltetrols (2-MTLs, 2-methylthreitol and 2-methylerythritol), 3-MeTHF-3,4-diols (*cis*-3-  
107 methyltetrahydrofuran-3,4-diol and *trans*-3-methyltetrahydrofuran-3,4-diol) and C<sub>5</sub>-alkene triols (*cis*-2-  
108 methyl-1,3,4-trihydroxy-1-butene, *trans*-2-methyl-1,3,4-trihydroxy-1-butene and 3-methyl-2,3,4-  
109 trihydroxy-1-butene). The monoterpenes-derived SOA (SOA<sub>M</sub>) tracers included 3-hydroxy-4,4-  
110 dimethylglutaric acid (HDMGA), 3-hydroxyglutaric acid (HGA), pinic acid (PA), *cis*-pinonic acid  
111 (PNA), and 3-methyl-1,2,3-butanetricarboxylic acid (MBTCA). The β-caryophyllene-derived SOA  
112 (SOA<sub>C</sub>) tracer was β-caryophyllenic acid (CA). Due to the lack of authentic standards, surrogate  
113 standards were used to quantify BSOA tracers except PNA. Specifically, erythritol, PNA and  
114 octadecanoic acid were used for the quantification of SOA<sub>I</sub> tracers (Ding et al., 2008), other SOA<sub>M</sub> tracers  
115 (Ding et al., 2014) and CA (Ding et al., 2011), respectively. The method detection limits (MDLs) for  
116 erythritol, PNA and octadecanoic acid were 0.01, 0.02, and 0.02 ng m<sup>-3</sup>, respectively. Table S1  
117 summarizes BSOA data at each site in the PRD.

### 118 2.3 Quality Assurance / Quality Control

119 These target BSOA tracers were not detected or lower than MDLs in the field blanks. The results of  
120 spiked samples (erythritol, PNA and octadecanoic acid spiked in pre-baked quartz filters) indicated that  
121 the recoveries were 65 ± 14 % for erythritol, 101 ± 3 % for PNA, and 83 ± 7 % for octadecanoic acid.  
122 The results of paired duplicate samples indicated that all the relative differences for target BSOA tracers  
123 were lower than 15%.

124 It should be noted that the application of surrogate quantification introduces additional errors to the  
125 results. Based on the empirical approach to calculate uncertainties from surrogate quantification (Stone  
126 et al., 2012), we estimated the errors in analyte measurement which were propagated from the  
127 uncertainties in field blanks, spike recoveries, repeatability and surrogate quantification. As Table S2  
128 showed, the estimated uncertainties in the tracers' measurement ranged from 15% (PNA) to 157% (CA).

## 129 3 Results and Discussion

### 130 3.1 PM<sub>2.5</sub> and gaseous pollutants

131 Figure 2 presents spatial and seasonal variations of PM<sub>2.5</sub> and its major components. Although annual-  
132 mean PM<sub>2.5</sub> (34.8 ± 6.1 μg m<sup>-3</sup>) in the PRD met the NAAQS value of 35 μg m<sup>-3</sup>, PM<sub>2.5</sub> at the urban sites



133 (ZQ, GZ and DG) all exceeded the NAAQS value. The rural TH site in the northern part of PRD  
134 witnessed the lowest concentration of  $PM_{2.5}$  ( $25.0 \mu\text{g m}^{-3}$ ) among the nine sites.  $PM_{2.5}$  levels were highest  
135 in winter (on average  $60.1 \pm 21.6 \mu\text{g m}^{-3}$ ) and lowest in summer (on average  $22.8 \pm 3.3 \mu\text{g m}^{-3}$ ).  
136 Carbonaceous aerosols and water-soluble ions together explained  $98 \pm 11 \%$  of  $PM_{2.5}$  masses. OM  
137 ( $OC \times 1.6$ ) was the most abundant component in  $PM_{2.5}$ , followed by sulfate, ammonium, nitrate and EC.  
138 Similar to  $PM_{2.5}$ , the five major components all increased in winter and fall (Figure S1), suggesting severe  
139  $PM_{2.5}$  pollution during fall-winter season in the PRD.

140 In the gas phase,  $SO_2$ , CO,  $NO_2$  and  $NO_x$  presented similar seasonal trends as  $PM_{2.5}$ , i.e. higher  
141 levels occurred during fall and winter and lower concentrations during spring and summer (Figure 3 a-  
142 d). Annual-mean  $SO_2$  and  $NO_2$  in the PRD both met the NAAQS values of  $60 \mu\text{g m}^{-3}$  and  $40 \mu\text{g m}^{-3}$ ,  
143 respectively (Figure 3a and 3c). As a typical secondary pollutant,  $O_3$  was highest in summer (Figure 3e),  
144 probably because of the strong photo-chemistry. Due to the compromise of opposite seasonal trends of  
145  $O_3$  and  $NO_2$ ,  $O_x$  showed less seasonal variation (Figure 3f) compared with other gaseous pollutants. And  
146 annual-mean  $O_x$  reached  $96.1 \pm 14.9 \mu\text{g m}^{-3}$ . These imply that atmospheric oxidative capacity is high all  
147 the year in the PRD.

### 148 3.2 Spatial distribution and seasonal variation of SOA tracers

149 The total concentrations of BSOA tracers ranged from  $45.4$  to  $109 \text{ ng m}^{-3}$  among the nine sites.  $SOA_M$   
150 tracers ( $47.2 \pm 9.29 \text{ ng m}^{-3}$ ) represented predominance, followed by  $SOA_I$  tracers ( $23.1 \pm 10.8 \text{ ng m}^{-3}$ ),  
151 and  $SOA_C$  tracer ( $3.85 \pm 1.75 \text{ ng m}^{-3}$ ).

#### 152 3.2.1 Monoterpenes-derived SOA tracers

153 Annual averages of total  $SOA_M$  tracers at the nine sites were in the range of  $26.5$  to  $57.4 \text{ ng m}^{-3}$  (Table  
154 S1). Figure 4 and Figure S2a show the spatial distribution of  $SOA_M$  tracers and monoterpene emissions  
155 in the PRD (Zheng et al., 2010). The highest concentration of  $SOA_M$  tracers was observed at the rural  
156 TH site where monoterpene emissions were high. Figure 4 also presents seasonal variations of  $SOA_M$   
157 tracers. At most sites, high levels occurred in summer and fall. Monoterpene emission rates are  
158 influenced by temperature and solar radiation (Guenther et al., 2012). Thus, high temperature and  
159 intensive solar radiation during summer and fall in the PRD (Zheng et al., 2010) could stimulate  
160 monoterpene emissions and then the  $SOA_M$  formation.



161 Among the five SOA<sub>M</sub> tracers, HGA ( $20.1 \pm 4.28 \text{ ng m}^{-3}$ ) showed the highest concentration,  
162 followed by HDMGA ( $14.7 \pm 2.93 \text{ ng m}^{-3}$ ), MBTCA ( $7.63 \pm 1.49 \text{ ng m}^{-3}$ ), PNA ( $3.75 \pm 2.72 \text{ ng m}^{-3}$ ) and  
163 PA ( $1.01 \pm 0.48 \text{ ng m}^{-3}$ ). SOA<sub>M</sub> formation undergoes multi-generation reactions. The first-generation  
164 SOA<sub>M</sub> (SOA<sub>M,F</sub>) products, PNA and PA, can be further oxidized and form the high-generation (SOA<sub>M,H</sub>)  
165 products, e.g. MBTCA (Müller et al., 2012). Thus, the (PNA+PA) / MBTCA ratio has been used to probe  
166 SOA<sub>M</sub> aging (Haque et al., 2016; Ding et al., 2014). The (PNA+PA) / MBTCA ratios in chamber-  
167 generated  $\alpha$ -pinene SOA samples were reported in the range of 1.51 to 5.91 depending on different  
168 oxidation conditions (Offenberg et al., 2007; Eddingsaas et al., 2012). In this study, the median values of  
169 (PNA+PA) / MBTCA varied from 0.27 at ZH to 1.67 at TH. The ratios observed in this study were  
170 consistent with our previous observations at the regional site, Wangqingsha (WQS) in the PRD (Ding et  
171 al., 2012), but lower than those in the fresh  $\alpha$ -pinene SOA samples from chamber experiments (Figure  
172 S3), indicating relatively aged SOA<sub>M</sub> in the air of PRD.

173 Moreover, the levels of SOA<sub>M,H</sub> tracers (HGA + HDMGA + MBTCA) were much higher than those  
174 of SOA<sub>M,F</sub> tracers (PNA + PA), with mean mass fractions of SOA<sub>M,H</sub> tracers reaching 86% (Figure 4).  
175 Mass fractions of SOA<sub>M,F</sub> tracers decreased in the summer samples (Figure 4), probably resulting from  
176 strong photo-chemistry and more intensive further oxidation during summer. High abundances of  
177 SOA<sub>M,H</sub> tracers in the PRD were different from our year-round observations at 12 sites across China  
178 (Ding et al., 2016b). In that study, the (PNA+PA) / MBTCA ratio suggested generally fresh SOA<sub>M</sub> (Figure  
179 S3) and SOA<sub>M,F</sub> tracers were the majority. Thus, we see more aged SOA<sub>M</sub> in the PRD.

180 As Figure 5 a-b showed, the SOA<sub>M,F</sub> tracers did not show good correlations with O<sub>x</sub> at most sites,  
181 while the SOA<sub>M,H</sub> tracers exhibited significant O<sub>x</sub> dependence. When atmospheric oxidation capacity is  
182 high, strong photo-oxidation of PNA and PA could reduce their concentrations and promote the formation  
183 of SOA<sub>M,H</sub> tracers (Müller et al., 2012). Thus, the levels of SOA<sub>M,H</sub> tracers would increase with  
184 increasing O<sub>x</sub> but not so for SOA<sub>M,F</sub> tracers. On the other hand, sulfate is a key species in particles that  
185 determines aerosol acidity and promotes SOA formation through the salting-in effect and heterogeneous  
186 reactions (Offenberg et al., 2009; Xu et al., 2016). The SOA<sub>M,F</sub> tracers poorly correlated with sulfate  
187 (Figure 5c), while the SOA<sub>M,H</sub> tracers presented significant sulfate dependence at all the 9 sites (Figure  
188 5d). This suggested that sulfate also played a critical role in forming SOA<sub>M,H</sub> tracers through particle  
189 phase reactions. Here, we conclude that high concentrations of O<sub>x</sub> and sulfate could stimulate SOA<sub>M,H</sub>  
190 tracers' production and thereby lead to aged SOA<sub>M</sub> in the PRD.



### 191 3.2.2 Isoprene-derived SOA tracers

192 Annual averages of total SOA<sub>1</sub> tracers at the nine sites were in the range of 10.8 to 49.3 ng m<sup>-3</sup> (Table  
193 S1). Figure 6 and Figure S2b show the spatial distribution of SOA<sub>1</sub> tracers and isoprene emissions in the  
194 PRD (Zheng et al., 2010), respectively. The highest concentration occurred at ZQ where the emissions  
195 were high. Figure 6 also presents seasonal variations of SOA<sub>1</sub> tracers at the nine sites. High levels  
196 occurred in summer and fall. Similar to monoterpenes, the emission rate of isoprene is influenced by  
197 temperature and solar radiation (Guenther et al., 2012), which are expected to be higher in summer and  
198 fall in the PRD (Zheng et al., 2010). Among these SOA<sub>1</sub> tracers, 2-MTLs (14.2 ± 5.61 ng m<sup>-3</sup>) were the  
199 most abundant products, followed by C<sub>5</sub>-alkene triols (6.81 ± 5.05 ng m<sup>-3</sup>), 2-MGA (1.99 ± 0.72 ng m<sup>-3</sup>)  
200 and 3-MeTHF-3,4-diols (0.19 ± 0.08 ng m<sup>-3</sup>).

201 SOA<sub>1</sub> formation is highly affected by NO<sub>x</sub> (Surratt et al., 2010). Under the low-NO<sub>x</sub> or NO<sub>x</sub> free  
202 conditions, isoprene is oxidized by the OH and HO<sub>2</sub> radicals through the HO<sub>2</sub>-channel which generates  
203 a hydroxy hydroperoxide (ISOPOOH) and then forms epoxydiols (IEPOX) (Paulot et al., 2009). Reactive  
204 uptake of IEPOX on acidic particles eventually produces 2-MTLs, C<sub>5</sub>-alkene triols, 3-MeTHF-3,4-diols,  
205 2-MTLs-organosulfates and oligomers (Lin et al., 2012). Under the high-NO<sub>x</sub> conditions, isoprene  
206 undergoes oxidation by NO<sub>x</sub> through the NO/NO<sub>2</sub>-channel and generates methacrolein (MACR) and then  
207 forms peroxyacetic nitric anhydride (MPAN). Further oxidation of MPAN by the OH radical  
208 produces hydroxymethyl-methyl- $\alpha$ -lactone (HMML) and/or methacrylic acid epoxide (MAE). HMML  
209 and MAE are the direct precursors to 2-MGA, 2-MGA-organosulfate and its corresponding oligomers  
210 (Nguyen et al., 2015). As Figure 6 showed, the concentrations of HO<sub>2</sub>-channel tracers (2-MTLs + C<sub>5</sub>-  
211 alkene triols + 3-MeTHF-3,4-diols) were much higher than those of the NO/NO<sub>2</sub>-channel product (2-  
212 MGA) at all the nine sites. The dominance of HO<sub>2</sub>-channel products was also observed at another  
213 regional site in the PRD (WQS), largely due to strong heterogeneous reactions of IEPOXs on the acidic  
214 particles in the polluted air (He et al., 2018).

215 Figure 6 also shows seasonal trends of the 2-MGA to 2-MTLs ratio (2-MGA/2-MTLs) which is  
216 often applied to probe the influence of NO<sub>x</sub> on the formation of SOA<sub>1</sub> (Ding et al., 2013; Ding et al.,  
217 2016a; Pye et al., 2013). The ratios were highest in wintertime and lowest in summertime, which were  
218 consistent with the seasonal trend of NO<sub>x</sub> during our campaign (Figure 3d). As Table 1 showed, 2-MGA  
219 positively correlated with NO<sub>2</sub>, probably due to the enhanced formation of MPAN from



220 peroxyacetyl (PAA) radical reacted with NO<sub>2</sub> (Worton et al., 2013; Chan et al., 2010). Previous  
221 laboratory studies showed that increasing NO<sub>2</sub>/NO ratio could promote the formation of 2-MGA and its  
222 corresponding oligoesters (Chan et al., 2010; Surratt et al., 2010). However, we did not see a significant  
223 correlation between 2-MGA and NO<sub>2</sub>/NO ratio in the PRD. Instead, the 2-MGA/2-MTLs ratio correlated  
224 well with NO, NO<sub>2</sub> and NO<sub>2</sub>/NO ratio (Table 1). Increasing NO limits the formation of ISOPOOH but  
225 prefers the production of MACR, and increasing NO<sub>2</sub> enhances MPAN formation. Thus, it is expected  
226 that the 2-MGA/2-MTLs ratio shows stronger NO<sub>x</sub> dependence than 2-MGA. These findings demonstrate  
227 the significant impact of NO<sub>x</sub> on SOA<sub>1</sub> formation pathways in the atmosphere.

228 Recent studies indicated that isoprene ozonolysis might play a role in SOA<sub>1</sub> formation in the ambient  
229 air. Riva et al. (2016) found that isoprene ozonolysis with acidic particles could produce substantial 2-  
230 MTLs but not so for C<sub>5</sub>-alkene triols and 3-MeTHF-3,4-diols. Li et al. (2018) observed a positive  
231 correlation between 2-MTLs and O<sub>3</sub> in the North China Plain. In the PRD, we also saw weak but  
232 significant correlations of 2-MTLs with O<sub>3</sub> (Table S3). However, 3-MeTHF-3,4-diols and C<sub>5</sub>-alkene  
233 triols were detected in all samples and 2-MTLs, C<sub>5</sub>-alkene triols and 3-MeTHF-3,4-diols correlated well  
234 with each other (Table S4), which was apparently different from those reported by Riva et al. (2016).  
235 Moreover, the ratios of 2-MTLs isomers in the PRD samples (2.00–2.85) were much lower than those  
236 (10–22, Figure S4) reported in the SOA from isoprene ozonolysis (Riva et al., 2016). Furthermore,  
237 isoprene oxidation by the OH radical is much faster than that by ozone under the polluted PRD conditions  
238 (Table S5). And IEPOX yields through the ISOPOOH oxidation by the OH radical are more than 75%  
239 in the atmosphere (St. Clair et al., 2016). Thus, isoprene ozonolysis might be not the major formation  
240 pathway of SOA<sub>1</sub>, even though annual-mean O<sub>3</sub> level reaching 67.7 μg m<sup>-3</sup> in the PRD (Table S1).

241 A previous study found that thermal decomposition of low volatility organics in IEPOX-derived  
242 SOA could produce SOA<sub>1</sub> tracers, e.g. 2-MTLs, C<sub>5</sub>-alkene triols and 3-MeTHF-3,4-diols (Lopez-Hilfiker  
243 et al., 2016). This means that these tracers detected by GC-MSD might be generated from thermal  
244 decomposition of IEPOX-derived SOA. If these tracers were mainly generated from such a thermal  
245 process, their compositions would be similar in different samples. To verify this possibility, we presented  
246 chemical compositions of three C<sub>5</sub>-alkene triol isomers at the nine sites in ternary plots. The relative  
247 abundances of three isomers significantly changed from site to site (Figure 7) and season to season  
248 (Figure S5), and were different from those measured in the chamber samples (Lin et al., 2012). Moreover,  
249 the slopes of linear correlations among these IEPOX-derived SOA tracers also varied from site to site



250 (Figure S6). Coupled with the seasonal trend of 2-MGA/2-MTLs ratios, the observed variations in SOA<sub>I</sub>  
251 tracers compositions demonstrated that the SOA<sub>I</sub> tracers were mainly formed through different pathways  
252 in the real atmosphere rather than thermal decomposition.

### 253 3.2.3 Sesquiterpene-derived SOA tracer

254 Annual averages of CA at the nine sites ranged from 1.82 to 7.07 ng m<sup>-3</sup>. The levels of CA at the inland  
255 sites (e.g. GZ, ZQ, and TH) were higher than those at the coastal sites (ZH and NS, Figure 8). Since  
256 sesquiterpenes are typical BVOCs, it is unexpected that the concentrations of CA were highest during  
257 winter in the PRD (Figure 8). Interestingly, seasonal trend of CA was consistent with that of the biomass  
258 burning (BB) tracer, levoglucosan (Figure 8). And CA correlated well with levoglucosan at eight sites in  
259 the PRD (Figure 9a). Sesquiterpenes are stored in plant tissues partly to protect the plants from insects  
260 and pathogens (Keeling and Bohlmann, 2006). BB can not only stimulate sesquiterpene emissions  
261 (Ciccioli et al., 2014) but also substantially alter the SOA formation and yields (Mentel et al., 2013).  
262 Emissions inventories in the PRD showed that the BB emissions were enhanced during winter (He et al.,  
263 2011). These suggested that the unexpected increase of SOA<sub>C</sub> in wintertime could be highly associated  
264 with BB emissions in the PRD.

265 Besides the impact of BB, we also found positive correlations of CA with O<sub>x</sub> (Figure 9b) and sulfate  
266 (Figure 9c). The oxidation of β-caryophyllene by the OH radical and O<sub>3</sub> is very rapid with the lifetimes  
267 less than 10 min under typical conditions in the air of PRD (Table S5). The increase of sulfate could not  
268 only raise aerosol acidity but also enhance the salting-in effect (Xu et al., 2015). In the PRD, both O<sub>x</sub>  
269 (Figure 3f) and sulfate (Figure S1) increased during winter, which could promote SOA<sub>C</sub> formation. Here,  
270 we conclude that the enhancement of BB emissions as well as the increase of O<sub>x</sub> and sulfate in wintertime  
271 together led to high SOA<sub>C</sub> production during winter in the PRD.

### 272 3.3 Source apportionment and atmospheric implications

273 We further attributed BSOA by the SOA-tracer approach which was first developed by Kleindienst et al.  
274 (2007). This method has applied to SOA apportionment at multiple sites across the United States  
275 (Lewandowski et al., 2013) and China (Ding et al., 2016b), and over global oceans from Arctic to  
276 Antarctic (Hu et al., 2013). Details of the SOA-tracer method and its application in this study as well as  
277 the uncertainty of estimating procedure are described in Text S1. Table S1 lists the results of estimated



278 SOA from different BVOCs.

279 Figure 10a exhibits the spatial distribution of BSOA ( $\text{SOA}_M + \text{SOA}_I + \text{SOA}_C$ ). Annual average at  
280 the nine sites ranged from  $0.97 \mu\text{g m}^{-3}$  (NS) to  $2.19 \mu\text{g m}^{-3}$  (ZQ), accounting for 9-15% of OM.  $\text{SOA}_M$   
281 was the largest BSOA contributor with an average contribution of  $64 \pm 7\%$ , followed by  $\text{SOA}_C$  ( $21 \pm$   
282  $6\%$ ), and  $\text{SOA}_I$  ( $14 \pm 4\%$ ). Figure 10b presents seasonal variation of BSOA. The levels were highest in  
283 fall ( $2.35 \pm 0.95 \mu\text{g m}^{-3}$ ) and lowest in spring ( $1.06 \pm 0.42 \mu\text{g m}^{-3}$ ).  $\text{SOA}_M$  contributions ranged from 57%  
284 in winter to 68% in spring. The shares of  $\text{SOA}_I$  were only 5% in winter and reached up to 22% in summer.  
285 The contributions of  $\text{SOA}_C$  increased to 40% in wintertime.

286 It is interesting to note that  $\text{SOA}_M$ ,  $\text{SOA}_I$  and  $\text{SOA}_C$  all positively correlated with sulfate and  $\text{O}_x$  in  
287 the PRD (Table 2). Anthropogenic emissions significantly influence BSOA formation (Carlton et al.,  
288 2018). The observed sulfate and  $\text{O}_x$  dependence of BSOA in the air of PRD indicates that the reduction  
289 of  $1 \mu\text{g m}^{-3}$  in sulfate and  $\text{O}_x$  could lower BSOA levels by  $0.17$  and  $0.02 \mu\text{g m}^{-3}$ , respectively. If both  
290 concentrations decline by 50%, the reduction of  $\text{O}_x$  is more efficient than sulfate in reducing BSOA in  
291 the PRD (Table 2). Due to strict control of  $\text{SO}_2$  emissions (Wang et al., 2013), ambient  $\text{SO}_2$  significantly  
292 shrank over the PRD (Figure 1b). However,  $\text{O}_x$  levels did not decrease during the past decade (Figure 1b)  
293 and  $\text{O}_x$  concentrations were much higher than sulfate in the PRD ( $96.1 \pm 14.9 \mu\text{g m}^{-3}$  vs.  $8.44 \pm 1.09 \mu\text{g}$   
294  $\text{m}^{-3}$  on average). At present, short-term despiking and long-term attainment of  $\text{O}_3$  concentrations are  
295 challenges for air pollution control in the PRD (Ou et al., 2016). Thus, lowering  $\text{O}_x$  is critical to improve  
296 air quality in the PRD. Our results highlight the importance of future reduction in anthropogenic pollutant  
297 emissions (e.g.  $\text{SO}_2$  and  $\text{O}_x$  precursors) for considerably reducing the BSOA burden in polluted regions.

#### 298 **Code/Data availability**

299 The experimental data in this study are available upon request to the corresponding author by email.

#### 300 **Author Contribution**

301 Xiang Ding, Duo-Hong Chen and Jun Li conceived the project and designed the study. Yu-Qing Zhang  
302 and Duo-Hong Chen performed the data analysis and wrote the manuscript. Duo-Hong Chen, Tao Zhang  
303 and Yu-Bo Ou arranged the sample collection and assisted with the data analysis. Jun-Qi Wang, Qian  
304 Cheng and Hao Jiang analyzed the samples. Xiang Ding, Peng-Lin Ye, Wei Song, Gan Zhang and Xin-



305 Ming Wang performed data interpretation and edited the manuscript. All authors contributed to the final  
306 manuscript development.

### 307 **Competing interests**

308 The authors declare that they have no conflict of interest.

### 309 **Acknowledgments**

310 This study was supported by National Key Research and Development Program (2018YFC0213902),  
311 National Natural Science Foundation of China (41722305/41603070/41473099), and Local Innovative  
312 and Research Teams Project of Guangdong Pearl River Talents Program (NO. 2017BT01Z134). The data  
313 of gaseous pollutants, major components in PM<sub>2.5</sub> and BSOA tracers can be found in supporting  
314 information.

### 315 **References**

- 316 Carlton, A. G., Pinder, R. W., Bhave, P. V., and Pouliot, G. A.: To what extent can biogenic SOA be  
317 controlled?, *Environ. Sci. Technol.*, 44, 3376-3380, 10.1021/es903506b, 2010.
- 318 Carlton, A. G., Pye, H. O. T., Baker, K. R., and Hennigan, C. J.: Additional benefits of federal air-quality  
319 rules: Model estimates of controllable biogenic secondary organic aerosol, *Environ. Sci. Technol.*, 52,  
320 9254-9265, 10.1021/acs.est.8b01869, 2018.
- 321 Chan, A. W. H., Chan, M. N., Surratt, J. D., Chhabra, P. S., Loza, C. L., Crounse, J. D., Yee, L. D., Flagan,  
322 R. C., Wennberg, P. O., and Seinfeld, J. H.: Role of aldehyde chemistry and NO<sub>x</sub> concentrations in  
323 secondary organic aerosol formation, *Atmos. Chem. Phys.*, 10, 7169-7188, 10.5194/acp-10-7169-  
324 2010, 2010.
- 325 Ciccioli, P., Centritto, M., and Loreto, F.: Biogenic volatile organic compound emissions from vegetation  
326 fires, *Plant. Cell. Environ.*, 37, 1810-1825, 10.1111/pce.12336, 2014.
- 327 Ding, X., Zheng, M., Yu, L., Zhang, X., Weber, R. J., Yan, B., Russell, A. G., Edgerton, E. S., and Wang,  
328 X.: Spatial and seasonal trends in biogenic secondary organic aerosol tracers and water-soluble organic  
329 carbon in the southeastern United States, *Environ. Sci. Technol.*, 42, 5171-5176, 10.1021/es7032636,  
330 2008.



- 331 Ding, X., Wang, X., and Zheng, M.: The influence of temperature and aerosol acidity on biogenic  
332 secondary organic aerosol tracers: Observations at a rural site in the central Pearl River Delta region,  
333 South China, *Atmos. Environ.*, 45, 1303-1311, 10.1016/j.atmosenv.2010.11.057, 2011.
- 334 Ding, X., Wang, X., Gao, B., Fu, X., He, Q., Zhao, X., Yu, J., and Zheng, M.: Tracer based estimation of  
335 secondary organic carbon in the Pearl River Delta, South China, *J. Geophys. Res-Atmos.*, 117, D05313,  
336 10.1029/2011JD016596, 2012.
- 337 Ding, X., Wang, X., Xie, Z., Zhang, Z., and Sun, L.: Impacts of Siberian biomass burning on organic  
338 aerosols over the North Pacific Ocean and the Arctic: Primary and secondary organic tracers, *Environ.*  
339 *Sci. Technol.*, 47, 3149-3157, 10.1021/es3037093, 2013.
- 340 Ding, X., He, Q. F., Shen, R. Q., Yu, Q. Q., and Wang, X. M.: Spatial distributions of secondary organic  
341 aerosols from isoprene, monoterpenes,  $\beta$ -caryophyllene, and aromatics over China during summer, *J.*  
342 *Geophys. Res-Atmos.*, 119, 11877-11891, 10.1002/2014JD021748, 2014.
- 343 Ding, X., He, Q. F., Shen, R. Q., Yu, Q. Q., Zhang, Y. Q., Xin, J. Y., Wen, T. X., and Wang, X. M.: Spatial  
344 and seasonal variations of isoprene secondary organic aerosol in China: Significant impact of biomass  
345 burning during winter, *Sci. Rep.*, 6, 20411, 10.1038/srep20411, 2016a.
- 346 Ding, X., Zhang, Y. Q., He, Q. F., Yu, Q. Q., Shen, R. Q., Zhang, Y., Zhang, Z., Lyu, S. J., Hu, Q. H.,  
347 Wang, Y. S., Li, L. F., Song, W., and Wang, X. M.: Spatial and seasonal variations of secondary organic  
348 aerosol from terpenoids over China, *J. Geophys. Res-Atmos.*, 121, 14661-14678,  
349 10.1002/2016JD025467, 2016b.
- 350 Donahue, N. M., Robinson, A. L., Stanier, C. O., and Pandis, S. N.: Coupled partitioning, dilution, and  
351 chemical aging of semivolatile organics, *Environ. Sci. Technol.*, 40, 2635-2643, 10.1021/es052297c,  
352 2006.
- 353 Eddingsaas, N. C., Loza, C. L., Yee, L. D., Chan, M., Schilling, K. A., Chhabra, P. S., Seinfeld, J. H., and  
354 Wennberg, P. O.:  $\alpha$ -pinene photooxidation under controlled chemical conditions – Part 2: SOA yield  
355 and composition in low- and high- $\text{NO}_x$  environments, *Atmos. Chem. Phys.*, 12, 7413-7427,  
356 10.5194/acp-12-7413-2012, 2012.
- 357 Guenther, A. B., Jiang, X., Heald, C. L., Sakulyanontvittaya, T., Duhl, T., Emmons, L. K., and Wang, X.:  
358 The model of emissions of gases and aerosols from nature version 2.1 (MEGAN2.1): an extended and  
359 updated framework for modeling biogenic emissions, *Geosci. Model. Dev.*, 5, 1471-1492,  
360 10.5194/gmd-5-1471-2012, 2012.



- 361 Haque, M. M., Kawamura, K., and Kim, Y.: Seasonal variations of biogenic secondary organic aerosol  
362 tracers in ambient aerosols from Alaska, *Atmos. Environ.*, 130, 95-104,  
363 10.1016/j.atmosenv.2015.09.075, 2016.
- 364 He, M., Zheng, J., Yin, S., and Zhang, Y.: Trends, temporal and spatial characteristics, and uncertainties  
365 in biomass burning emissions in the Pearl River Delta, China, *Atmos. Environ.*, 45, 4051-4059,  
366 10.1016/j.atmosenv.2011.04.016, 2011.
- 367 He, Q. F., Ding, X., Fu, X. X., Zhang, Y. Q., Wang, J. Q., Liu, Y. X., Tang, M. J., Wang, X. M., and  
368 Rudich, Y.: Secondary organic aerosol formation from isoprene epoxides in the Pearl River Delta,  
369 South China: IEPOX - and HMML - derived tracers, *J. Geophys. Res-Atmos.*, 123, 6999-7012,  
370 10.1029/2017JD028242, 2018.
- 371 Hofzumahaus, A., Rohrer, F., Lu, K., Bohn, B., Brauers, T., Chang, C.-C., Fuchs, H., Holland, F., Kita,  
372 K., Kondo, Y., Li, X., Lou, S., Shao, M., Zeng, L., Wahner, A., and Zhang, Y.: Amplified trace gas  
373 removal in the troposphere, *Science*, 324, 1702-1704, 10.1126/science.1164566, 2009.
- 374 Hoyle, C. R., Boy, M., Donahue, N. M., Fry, J. L., Glasius, M., Guenther, A., Hallar, A. G., Huff Hartz,  
375 K., Petters, M. D., Petäjä, T., Rosenoern, T., and Sullivan, A. P.: A review of the anthropogenic  
376 influence on biogenic secondary organic aerosol, *Atmos. Chem. Phys.*, 11, 321-343, 10.5194/acp-11-  
377 321-2011, 2011.
- 378 Hu, Q. H., Xie, Z. Q., Wang, X. M., Kang, H., He, Q. F., and Zhang, P.: Secondary organic aerosols over  
379 oceans via oxidation of isoprene and monoterpenes from Arctic to Antarctic, *Sci. Rep.*, 3, 2280,  
380 10.1038/srep02280, 2013.
- 381 Keeling, C. I., and Bohlmann, J.: Genes, enzymes and chemicals of terpenoid diversity in the constitutive  
382 and induced defence of conifers against insects and pathogens, *New. Phytol.*, 170, 657-675,  
383 10.1111/j.1469-8137.2006.01716.x, 2006.
- 384 Kleindienst, T. E., Jaoui, M., Lewandowski, M., Offenberg, J. H., Lewis, C. W., Bhawe, P. V., and Edney,  
385 E. O.: Estimates of the contributions of biogenic and anthropogenic hydrocarbons to secondary organic  
386 aerosol at a southeastern US location, *Atmos. Environ.*, 41, 8288-8300,  
387 10.1016/j.atmosenv.2007.06.045, 2007.
- 388 Lewandowski, M., Piletic, I. R., Kleindienst, T. E., Offenberg, J. H., Beaver, M. R., Jaoui, M., Docherty,  
389 K. S., and Edney, E. O.: Secondary organic aerosol characterisation at field sites across the United  
390 States during the spring–summer period, *Int. J. Environ. An. Ch.*, 93, 1084-1103,



- 391 10.1080/03067319.2013.803545, 2013.
- 392 Li, J., Wang, G., Wu, C., Cao, C., Ren, Y., Wang, J., Li, J., Cao, J., Zeng, L., and Zhu, T.: Characterization  
393 of isoprene-derived secondary organic aerosols at a rural site in North China Plain with implications  
394 for anthropogenic pollution effects, *Sci. Rep.*, 8, 535, 10.1038/s41598-017-18983-7, 2018.
- 395 Lin, Y.-H., Zhang, Z., Docherty, K. S., Zhang, H., Budisulistiorini, S. H., Rubitschun, C. L., Shaw, S.,  
396 Knipping, E., Edgerton, E. S., Kleindienst, T. E., Gold, A., and Surratt, J. D.: Isoprene epoxydiols as  
397 precursors to secondary organic aerosol formation: Acid-catalyzed reactive uptake studies with  
398 authentic standards, *Environ. Sci. Technol.*, 46, 189-195, 10.1021/es202554c, 2012.
- 399 Lopez-Hilfiker, F. D., Mohr, C., D'Ambro, E. L., Lutz, A., Riedel, T. P., Gaston, C. J., Iyer, S., Zhang,  
400 Z., Gold, A., Surratt, J. D., Lee, B. H., Kurten, T., Hu, W. W., Jimenez, J., Hallquist, M., and Thornton,  
401 J. A.: Molecular composition and volatility of organic aerosol in the southeastern U.S.: Implications  
402 for IEPOX derived SOA, *Environ. Sci. Technol.*, 50, 2200-2209, 10.1021/acs.est.5b04769, 2016.
- 403 Lu, Q., Zheng, J., Ye, S., Shen, X., Yuan, Z., and Yin, S.: Emission trends and source characteristics of  
404 SO<sub>2</sub>, NO<sub>x</sub>, PM<sub>10</sub> and VOCs in the Pearl River Delta region from 2000 to 2009, *Atmos. Environ.*, 76,  
405 11-20, 10.1016/j.atmosenv.2012.10.062, 2013.
- 406 Müller, L., Reinnig, M. C., Naumann, K. H., Saathoff, H., Mentel, T. F., Donahue, N. M., and Hoffmann,  
407 T.: Formation of 3-methyl-1,2,3-butanetricarboxylic acid via gas phase oxidation of pinonic acid – a  
408 mass spectrometric study of SOA aging, *Atmos. Chem. Phys.*, 12, 1483-1496, 10.5194/acp-12-1483-  
409 2012, 2012.
- 410 Mentel, T. F., Kleist, E., Andres, S., Maso, M. D., Hohaus, T., Kiendler-Scharr, A., Rudich, Y., Springer,  
411 M., Tillmann, R., Uerlings, R., Wahner, A., and Wildt, J.: Secondary aerosol formation from stress-  
412 induced biogenic emissions and possible climate feedbacks, *Atmos. Chem. Phys.*, 13, 8755-8770,  
413 10.5194/acp-13-8755-2013, 2013.
- 414 Nguyen, T. B., Bates, K. H., Crounse, J. D., Schwantes, R. H., Zhang, X., Kjaergaard, H. G., Surratt, J.  
415 D., Lin, P., Laskin, A., Seinfeld, J. H., and Wennberg, P. O.: Mechanism of the hydroxyl radical  
416 oxidation of methacryloyl peroxyxynitrate (MPAN) and its pathway toward secondary organic aerosol  
417 formation in the atmosphere, *Phys. Chem. Chem. Phys.*, 17, 17914-17926, 10.1039/C5CP02001H,  
418 2015.
- 419 Offenberg, J. H., Lewis, C. W., Lewandowski, M., Jaoui, M., Kleindienst, T. E., and Edney, E. O.:  
420 Contributions of toluene and  $\alpha$ -pinene to SOA formed in an irradiated toluene/ $\alpha$ -pinene/NO<sub>x</sub>/ air



- 421 mixture: Comparison of results using  $^{14}\text{C}$  content and SOA organic tracer methods, *Environ. Sci.*  
422 *Technol.*, 41, 3972-3976, 10.1021/es070089+, 2007.
- 423 Offenberg, J. H., Lewandowski, M., Edney, E. O., Kleindienst, T. E., and Jaoui, M.: Influence of aerosol  
424 acidity on the formation of secondary organic aerosol from biogenic precursor hydrocarbons, *Environ.*  
425 *Sci. Technol.*, 43, 7742–7747, 10.1021/es901538e, 2009.
- 426 Ou, J., Yuan, Z., Zheng, J., Huang, Z., Shao, M., Li, Z., Huang, X., Guo, H., and Louie, P. K. K.: Ambient  
427 ozone control in a photochemically active region: Short-term despiking or long-term attainment?,  
428 *Environ. Sci. Technol.*, 50, 5720–5728, 10.1021/acs.est.6b00345, 2016.
- 429 Paulot, F., Crouse, J. D., Kjaergaard, H. G., Kürten, A., St. Clair, J. M., Seinfeld, J. H., and Wennberg,  
430 P. O.: Unexpected epoxide formation in the gas-phase photooxidation of isoprene, *Science*, 325, 730-  
431 733, 10.1126/science.1172910, 2009.
- 432 Pye, H. O. T., Pinder, R. W., Piletic, I. R., Xie, Y., Capps, S. L., Lin, Y.-H., Surratt, J. D., Zhang, Z., Gold,  
433 A., Luecken, D. J., Hutzell, W. T., Jaoui, M., Offenberg, J. H., Kleindienst, T. E., Lewandowski, M.,  
434 and Edney, E. O.: Epoxide pathways improve model predictions of isoprene markers and reveal key  
435 role of acidity in aerosol formation, *Environ. Sci. Technol.*, 47, 11056-11064, 10.1021/es402106h,  
436 2013.
- 437 Riva, M., Budisulistiorini, S. H., Zhang, Z., Gold, A., and Surratt, J. D.: Chemical characterization of  
438 secondary organic aerosol constituents from isoprene ozonolysis in the presence of acidic aerosol,  
439 *Atmos. Environ.*, 130, 5-13, 10.1016/j.atmosenv.2015.06.027, 2016.
- 440 Riva, M., Budisulistiorini, S. H., Zhang, Z., Gold, A., Thornton, J. A., Turpin, B. J., and Surratt, J. D.:  
441 Multiphase reactivity of gaseous hydroperoxide oligomers produced from isoprene ozonolysis in the  
442 presence of acidified aerosols, *Atmos. Environ.*, 152, 314-322, 10.1016/j.atmosenv.2016.12.040, 2017.
- 443 Shen, R. Q., Ding, X., He, Q. F., Cong, Z. Y., Yu, Q. Q., and Wang, X. M.: Seasonal variation of secondary  
444 organic aerosol tracers in Central Tibetan Plateau, *Atmos. Chem. Phys.*, 15, 8781-8793, 10.5194/acp-  
445 15-8781-2015, 2015.
- 446 Sipilä, M., Jokinen, T., Berndt, T., Richters, S., Makkonen, R., Donahue, N. M., Mauldin Iii, R. L., Kurtén,  
447 T., Paasonen, P., Sarnela, N., Ehn, M., Junninen, H., Rissanen, M. P., Thornton, J., Stratmann, F.,  
448 Herrmann, H., Worsnop, D. R., Kulmala, M., Kerminen, V. M., and Petäjä, T.: Reactivity of stabilized  
449 Criegee intermediates (sCIs) from isoprene and monoterpene ozonolysis toward  $\text{SO}_2$  and organic acids,  
450 *Atmos. Chem. Phys.*, 14, 12143-12153, 10.5194/acp-14-12143-2014, 2014.



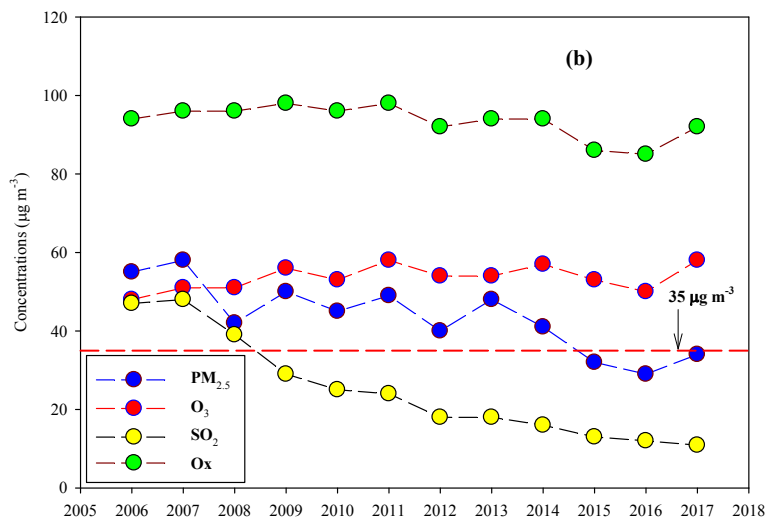
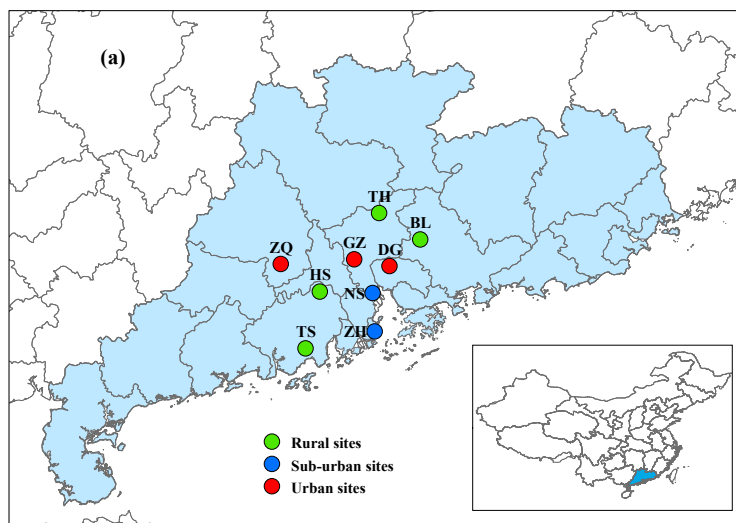
- 451 St. Clair, J. M., Rivera-Rios, J. C., Crounse, J. D., Knap, H. C., Bates, K. H., Teng, A. P., Jørgensen, S.,  
452 Kjaergaard, H. G., Keutsch, F. N., and Wennberg, P. O.: Kinetics and products of the reaction of the  
453 first-generation isoprene hydroxy hydroperoxide (ISOPOOH) with OH, *J. Phys. Chem. A*, 120, 1441-  
454 1451, 10.1021/acs.jpca.5b06532, 2016.
- 455 Stone, E. A., Nguyen, T. T., Pradhan, B. B., and Man Dangol, P.: Assessment of biogenic secondary  
456 organic aerosol in the Himalayas, *Environ. Chem.*, 9, 263-272, 10.1071/EN12002, 2012.
- 457 Surratt, J. D., Chan, A. W. H., Eddingsaas, N. C., Chan, M., Loza, C. L., Kwan, A. J., Hersey, S. P.,  
458 Flagan, R. C., Wennberg, P. O., and Seinfeld, J. H.: Reactive intermediates revealed in secondary  
459 organic aerosol formation from isoprene, *P. Natl. Acad. Sci. USA.*, 107, 6640-6645,  
460 10.1073/P.Natl.Acad.Sci.USA.0911114107, 2010.
- 461 Von Schneidemesser, E., Monks, P. S., Allan, J. D., Bruhwiler, L., Forster, P., Fowler, D., Lauer, A.,  
462 Morgan, W. T., Paasonen, P., Righi, M., Sindelarova, K., and Sutton, M. A.: Chemistry and the linkages  
463 between air quality and climate change, *Chem. Rev.*, 115, 3856-3897, 10.1021/acs.chemrev.5b00089,  
464 2015.
- 465 Wang, X., Liu, H., Pang, J., Carmichael, G., He, K., Fan, Q., Zhong, L., Wu, Z., and Zhang, J.: Reductions  
466 in sulfur pollution in the Pearl River Delta region, China: Assessing the effectiveness of emission  
467 controls, *Atmos. Environ.*, 76, 113-124, 10.1016/j.atmosenv.2013.04.074, 2013.
- 468 Worton, D. R., Surratt, J. D., LaFranchi, B. W., Chan, A. W. H., Zhao, Y., Weber, R. J., Park, J.-H.,  
469 Gilman, J. B., de Gouw, J., Park, C., Schade, G., Beaver, M., Clair, J. M. S., Crounse, J., Wennberg,  
470 P., Wolfe, G. M., Harrold, S., Thornton, J. A., Farmer, D. K., Docherty, K. S., Cubison, M. J., Jimenez,  
471 J.-L., Frossard, A. A., Russell, L. M., Kristensen, K., Glasius, M., Mao, J., Ren, X., Brune, W., Browne,  
472 E. C., Pusede, S. E., Cohen, R. C., Seinfeld, J. H., and Goldstein, A. H.: Observational insights into  
473 aerosol formation from isoprene, *Environ. Sci. Technol.*, 47, 11396–11402, 10.1021/es4011064, 2013.
- 474 Xu, L., Guo, H., Boyd, C. M., Klein, M., Bougiatioti, A., Cerully, K. M., Hite, J. R., Isaacman-VanWertz,  
475 G., Kreisberg, N. M., Knute, C., Olson, K., Koss, A., Goldstein, A. H., Hering, S. V., de Gouw, J.,  
476 Baumann, K., Lee, S.-H., Nenes, A., Weber, R. J., and Ng, N. L.: Effects of anthropogenic emissions  
477 on aerosol formation from isoprene and monoterpenes in the southeastern United States, *P. Natl. Acad.*  
478 *Sci. USA.*, 112, 37-42, 10.1073/P.Natl.Acad.Sci.USA.1417609112, 2015.
- 479 Xu, L., Middlebrook, A. M., Liao, J., de Gouw, J. A., Guo, H., Weber, R. J., Nenes, A., Lopez-Hilfiker,  
480 F. D., Lee, B. H., Thornton, J. A., Brock, C. A., Neuman, J. A., Nowak, J. B., Pollack, I. B., Welti, A.,



- 481 Graus, M., Warneke, C., and Ng, N. L.: Enhanced formation of isoprene-derived organic aerosol in  
482 sulfur-rich power plant plumes during Southeast Nexus, *J. Geophys. Res-Atmos.*, 121, 11137-11153,  
483 10.1002/2016JD025156, 2016.
- 484 Zhang, R. Y., Wang, G. H., Guo, S., Zarnora, M. L., Ying, Q., Lin, Y., Wang, W. G., Hu, M., and Wang,  
485 Y.: Formation of urban fine particulate matter, *Chem. Rev.*, 115, 3803-3855,  
486 10.1021/acs.chemrev.5b00067, 2015.
- 487 Zheng, J., Zheng, Z., Yu, Y., and Zhong, L.: Temporal, spatial characteristics and uncertainty of biogenic  
488 VOC emissions in the Pearl River Delta region, China, *Atmos. Environ.*, 44, 1960-1969,  
489 10.1016/j.atmosenv.2010.03.001, 2010.
- 490



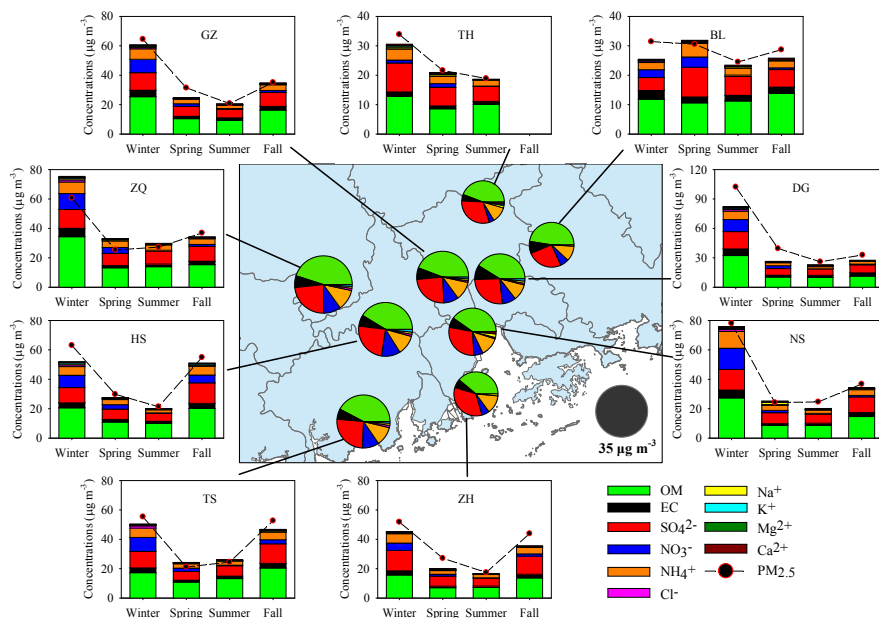
491



492

493 Figure 1 Sampling sites in the PRD (a) and long-term trends of annual-mean  $PM_{2.5}$ ,  $O_3$ ,  $SO_2$  and  $O_x$  recorded by the  
494 Guangdong-Hong Kong-Macao regional air quality monitoring network (<http://www.gdep.gov.cn/hjce/>) (b). The  
495 red dash line indicates the NAAQS for annual-mean  $PM_{2.5}$  concentrations ( $35 \mu g m^{-3}$ ).

496



497

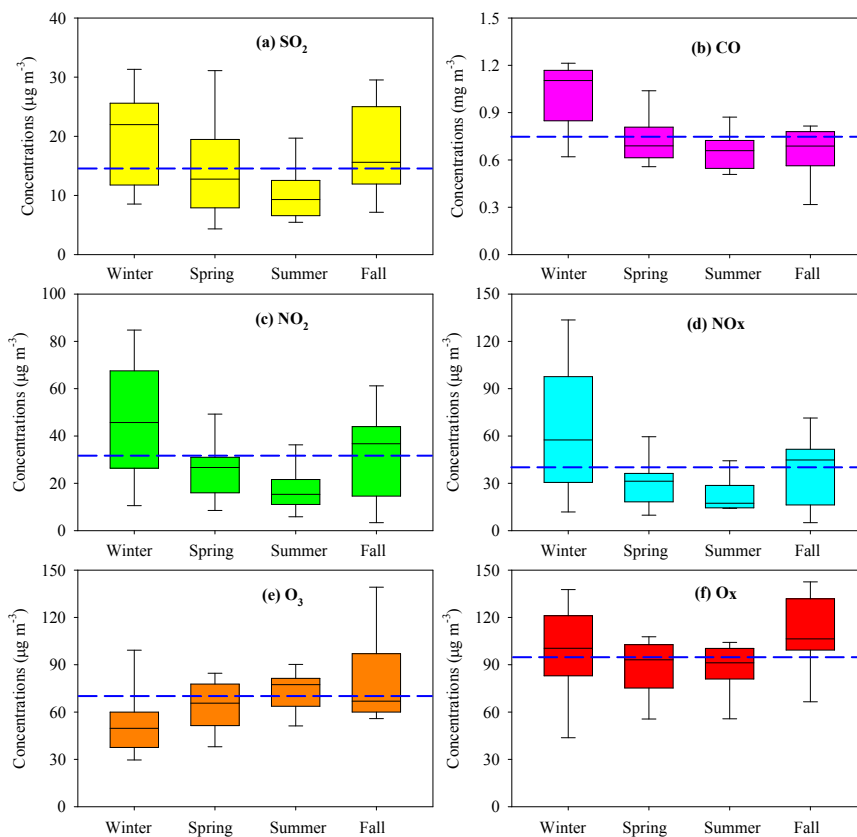
498

499

500

501

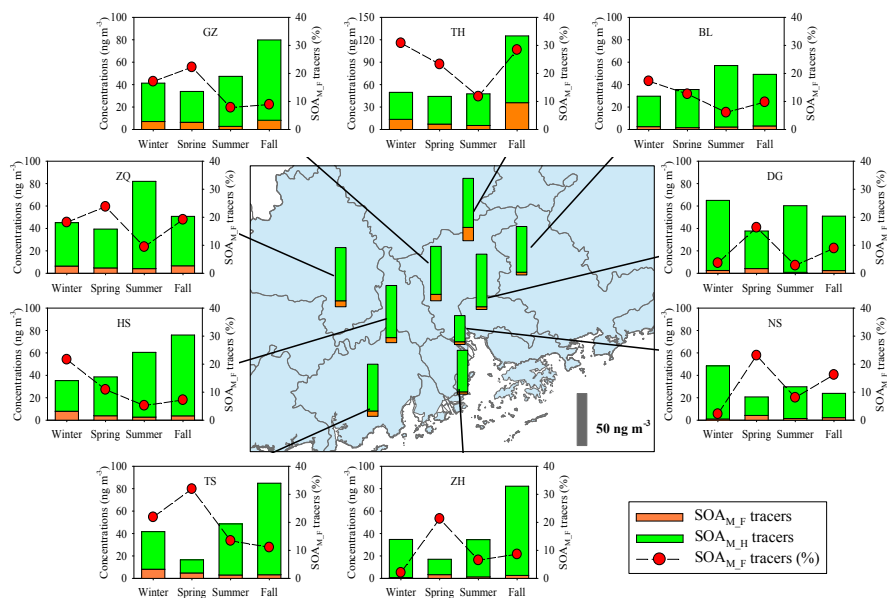
Figure 2 Major components in  $PM_{2.5}$  and their seasonal variation at 9 sites. The pie charts in the central figure represent the annual average of major components. High levels of  $PM_{2.5}$  and major components were observed in wintertime.



502

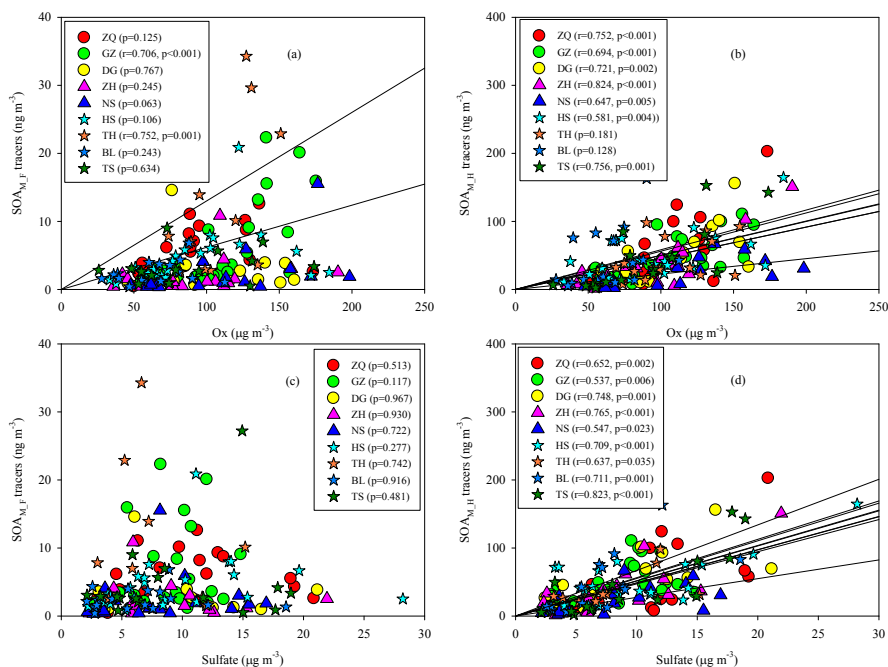
503 Figure 3 Seasonal variation of gaseous pollutants in the PRD. Box with error bars represent 10<sup>th</sup>, 25<sup>th</sup>, 75<sup>th</sup>, 90<sup>th</sup>  
504 percentiles for each pollutant. The line in each box represents the median value. Blue dash lines indicate annual  
505 average concentrations of  $\text{SO}_2$  (14.9  $\mu\text{g m}^{-3}$ ), CO (0.74  $\text{mg m}^{-3}$ ),  $\text{NO}_2$  (28.5  $\mu\text{g m}^{-3}$ ),  $\text{NO}_x$  (39.0  $\mu\text{g m}^{-3}$ ),  $\text{O}_3$  (67.7  $\mu\text{g}$   
506  $\text{m}^{-3}$ ) and  $\text{O}_x$  (96.1  $\mu\text{g m}^{-3}$ ).

507



508  
 509 Figure 4 Spatial and seasonal variations of SOAM tracers at 9 sites in the PRD. The bars in the central figure represent  
 510 the annual average concentrations of the SOAM tracers.

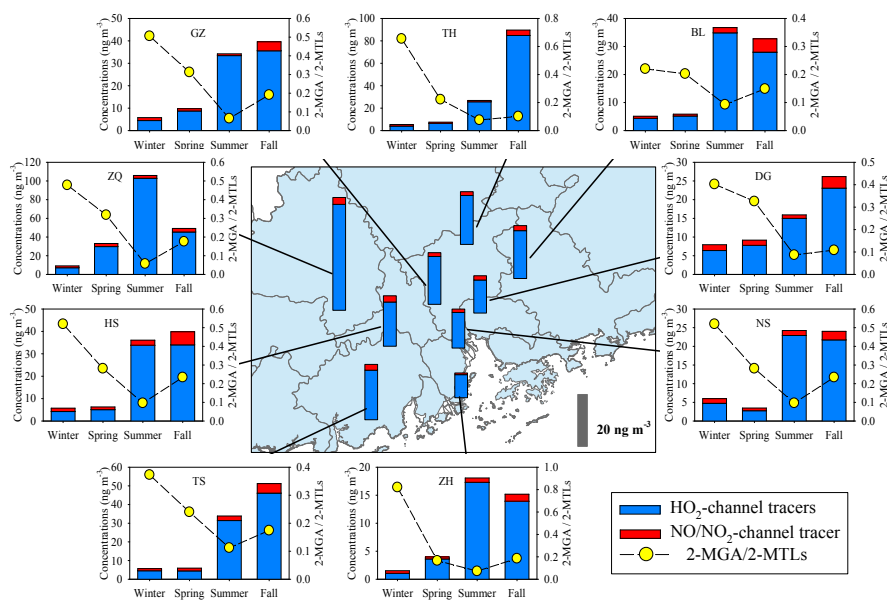
511



512

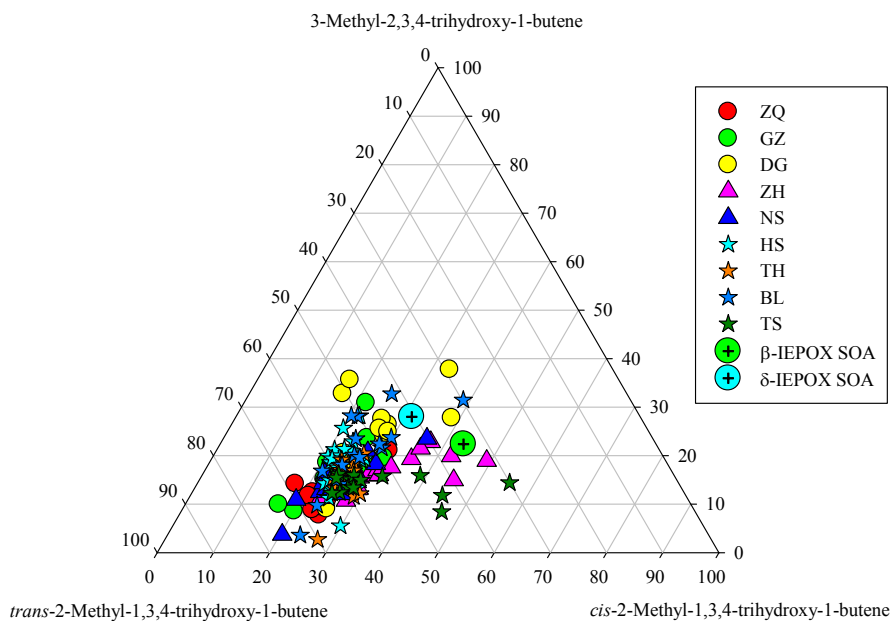
513 Figure 5 Correlations of SOA<sub>M,F</sub> and SOA<sub>M,H</sub> tracers with Ox (a, b) and sulfate (c, d)

514



515  
516 Figure 6 Spatial and seasonal variations of SOA<sub>1</sub> tracers at 9 sites in the PRD. The bars in the central figure represent  
517 the annual average concentrations of the SOA<sub>1</sub> tracers.

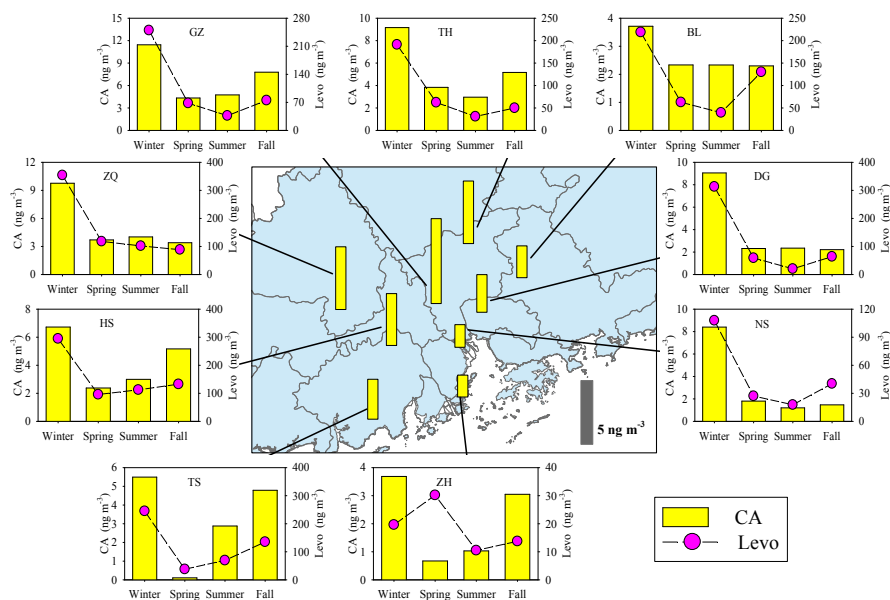
518



519

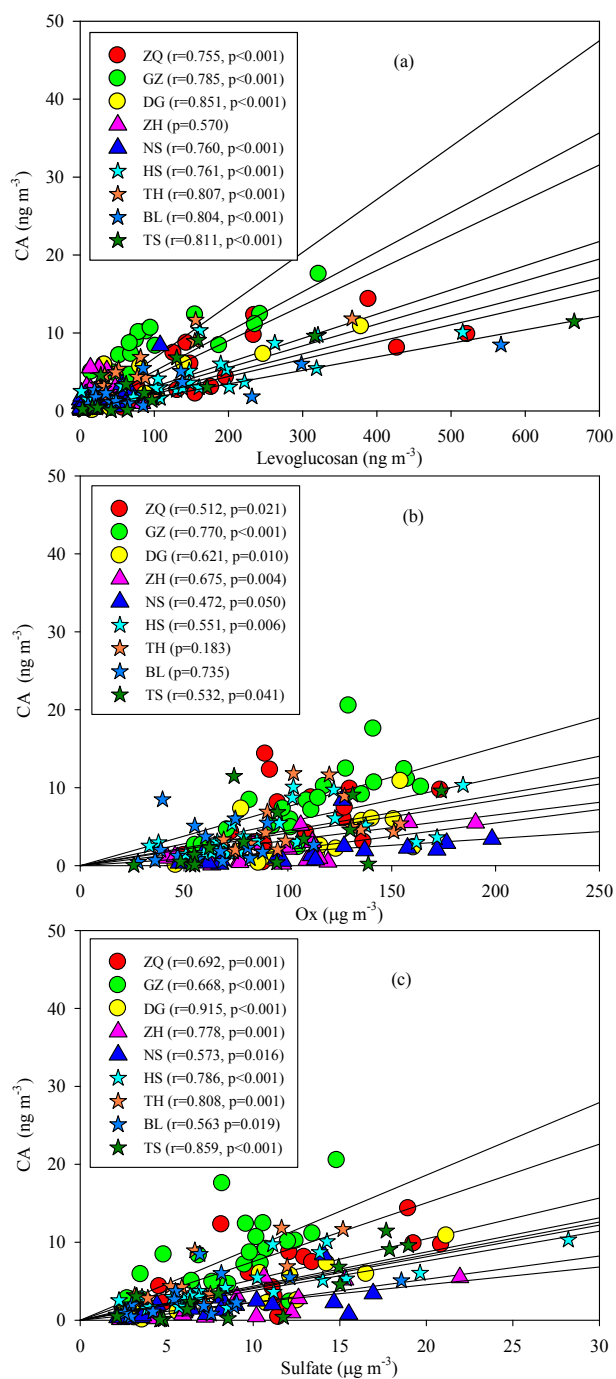
520 Figure 7 Ternary plot of C<sub>5</sub>-alkene triol isomers in the PRD samples and in the β-IEPOX and δ-IEPOX derived  
521 SOA (Lin et al., 2012).

522



523  
 524 Figure 8 Spatial and seasonal variations of SOA<sub>c</sub> tracer (CA) at 9 sites in the PRD. The bars in the central figure  
 525 represent the annual average concentration of the SOA<sub>c</sub> tracers. The pink circle indicates the BB tracer, levoglucosan  
 526 (Levo).

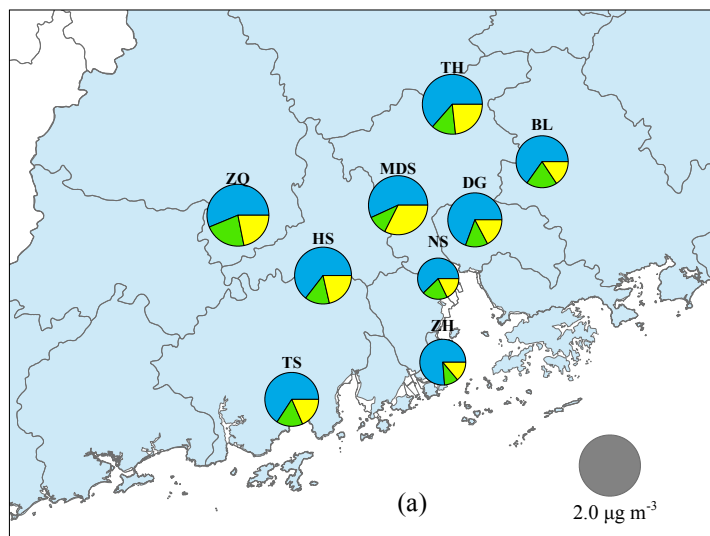
527



528

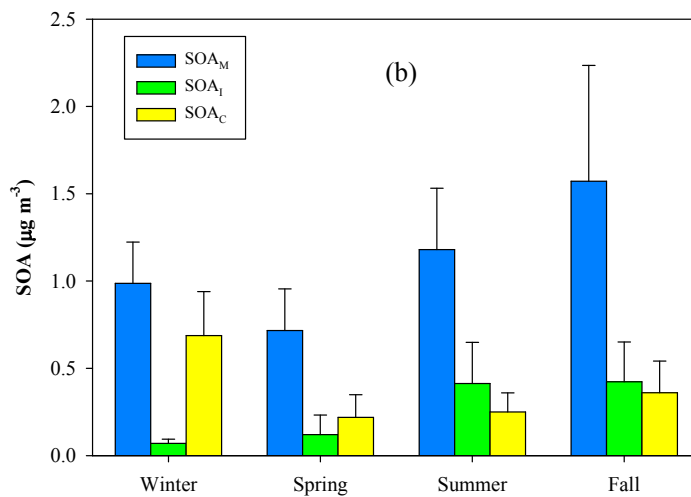
529 Figure 9 Significant correlations of CA with levoglucosan (a), Ox (b) and sulfate (c).

530



531

532



533

534 Figure 10 Spatial (a) and seasonal variations (b) of BSOA

535



536 Table 1 Correlations between SOA<sub>I</sub> tracers and NO<sub>x</sub>

	2-MGA		2-MGA/2-MTLs	
	Coefficient (r)	<i>p</i> -value	Coefficient (r)	<i>p</i> -value
NO	0.028	0.733	0.166	0.043
NO <sub>2</sub>	0.205	0.008	0.352	<0.001
NO <sub>x</sub>	0.132	0.102	0.286	<0.001
NO <sub>2</sub> /NO	0.001	0.986	0.162	0.048

537

538

539 Table 2 Correlations of BSOA with sulfate and O<sub>x</sub>

	Sulfate			O <sub>x</sub>		
	Slope	<i>p</i> -value	% <sup>a</sup>	Slope	<i>p</i> -value	% <sup>a</sup>
SOA <sub>M</sub>	0.112	<0.001	45	0.013	<0.001	57
SOA <sub>I</sub>	0.020	<0.001	34	0.003	<0.001	50
SOA <sub>C</sub>	0.041	<0.001	46	0.004	<0.001	55
BSOA	0.172	<0.001	44	0.019	<0.001	55

540 <sup>a</sup> Percentages of SOA reduction at 50% decline of sulfate or O<sub>x</sub>

541